

# Strong Support for the Millisecond Pulsar Origin of the Galactic Center GeV Excess

Richard Bartels,<sup>1,\*</sup> Suraj Krishnamurthy,<sup>1,†</sup> and Christoph Weniger<sup>1,‡</sup>

<sup>1</sup>*GRAPPA Institute, University of Amsterdam, Science Park 904, 1090 GL Amsterdam, Netherlands*

(Dated: 4 February 2016)

Using  $\gamma$ -ray data from the *Fermi* Large Area Telescope, various groups have identified a clear excess emission in the Inner Galaxy, at energies around a few GeV. This excess resembles remarkably well a signal from dark-matter annihilation. One of the most compelling astrophysical interpretations is that the excess is caused by the combined effect of a previously undetected population of dim  $\gamma$ -ray sources. Because of their spectral similarity, the best candidates are millisecond pulsars. Here, we search for this hypothetical source population, using a novel approach based on wavelet decomposition of the  $\gamma$ -ray sky and the statistics of Gaussian random fields. Using almost seven years of *Fermi*-LAT data, we detect a clustering of photons as predicted for the hypothetical population of millisecond pulsar, with a statistical significance of  $10.0\sigma$ . For plausible values of the luminosity function, this population explains 100% of the observed excess emission. We argue that other extragalactic or Galactic sources, a mismodeling of Galactic diffuse emission, or the thick-disk population of pulsars are unlikely to account for this observation.

*Introduction.* Since its launch in 2008, the *Fermi* Large Area Telescope (LAT) has revolutionized our understanding of the  $\gamma$ -ray sky. Among the major successes are the detection of more than 3000  $\gamma$ -ray sources [1], the discovery of the *Fermi* bubbles [2], some of the most stringent limits on dark-matter annihilation [3] and, most recently, the detection of cross-correlations between the extragalactic  $\gamma$ -ray background and various galaxy catalogs [4].

One of the most interesting  $\gamma$ -ray signatures identified in the *Fermi*-LAT data by various groups [5–16], is an excess emission in the Inner Galaxy at energies around a few GeV. This excess attracted great attention because it has properties typical for a dark-matter annihilation signal. This Galactic center excess (GCE) is detected both within the inner 10 arcmin of the Galactic Center (GC) [7, 9, 10] and up to Galactic latitudes of more than  $10^\circ$  [13, 15, 17, 18]. It features a remarkably uniform spectrum and approximately spherical symmetry [13, 15]. Proposed diffuse emission mechanisms, like leptonic or hadronic outbursts [19–21] or cosmic-ray injection in the central molecular zone [22], potentially explain part of the excess emission. However, it is challenging to explain *all* of the above aspects of the GCE with these mechanisms alone.

Probably the most plausible astrophysical interpretation for the GCE is the combined emission from a large number of unresolved millisecond pulsars (MSPs) in the Galactic bulge region [10, 12, 23, 24]. MSPs feature a spectrum compatible with the GCE emission [15], and a large unresolved component can naturally explain the uniformity of the GCE spectrum in different regions of the sky. Recently, it was shown that the spatial distribution of MSPs that were spilled out of disrupted globular clusters can explain the morphology of the GCE [25]. Such MSPs from disrupted globular clusters have also been suggested as the source behind the GeV through TeV emission in the inner few parsec of the GC [26]. Fur-

ther possible support for the MSP hypothesis might come from *Chandra* observations of low-mass x-ray binaries (which are progenitor systems of MSPs) in M31, which show a centrally peaked profile in the inner 2 kpc [27, 28], as well as the recent observation of extended hard X-ray emission from the Galactic Center by *NuSTAR* [29].

It was claimed that an interpretation of 100% of the GCE emission in terms of MSPs would be already ruled out: a sizeable fraction of the required  $10^3$ – $10^4$  MSPs should have been already detected by the *Fermi*-LAT [30, 31], but no (isolated) MSP has been identified so far in the bulge region. This conclusion depends crucially, however, on the adopted  $\gamma$ -ray luminosity of the brightest MSPs in the bulge population, on the effective source sensitivity of *Fermi*-LAT, and on the treatment of unassociated sources in the Inner Galaxy [25, 32]. A realistic sensitivity study for MSPs in the context of the GeV excess, taking into account all these effects, was lacking in the literature up to now (but see Ref. [33]).

In this Letter, we close this gap and present a novel technique for the analysis of dim  $\gamma$ -ray sources and apply it to *Fermi*-LAT observations of the Inner Galaxy. Our method is based on the statistics of maxima in the wavelet-transformed  $\gamma$ -ray sky (in context of *Fermi*-LAT data, wavelet transforms were used previously for the identification of point source seeds [1, 16]). We search for contributions from a large number of dim MSP-like sources, assuming that they are spatially distributed as suggested by GCE observations. Our method has several advantages with respect to previously proposed techniques based on one-point fluctuations [34], most notably the independence from Galactic diffuse emission models and the ability for candidate source localization.

*Modeling.* We simulate a population of MSP-like sources, which we hereafter refer to simply as the central source population (CSP), distributed around the GC at 8.5 kpc distance from the Sun. The CSP is taken to have a spatial distribution that follows a radial power law

with an index of  $\Gamma = -2.5$  and a hard cutoff at radius  $r = 3$  kpc [13, 15]. As a reference  $\gamma$ -ray energy spectrum, we adopt the stacked MSP spectrum from Ref. [35],  $\frac{dN}{dE} \propto e^{-E/3.78 \text{ GeV}} E^{-1.57}$ . The  $\gamma$ -ray luminosity function is modeled with a power law,  $\frac{dN}{dL} \propto L^{-\alpha}$ , with index  $\alpha = -1.5$  [32, 35–37], and with lower and upper hard cutoffs at  $L_{\min} = 10^{29} \text{ erg s}^{-1}$  and  $L_{\max} = 10^{34} - 10^{36} \text{ erg s}^{-1}$ , respectively. Luminosities are integrated over 0.1–100 GeV. Our results depend little on  $L_{\min}$ . Given that only about 70 MSPs have been detected in  $\gamma$  rays up to now [33],  $L_{\max}$  is not well constrained. The  $\gamma$ -ray luminosity of the brightest observed MSP is somewhere in the range  $(0.5-2) \times 10^{35} \text{ erg s}^{-1}$  [33, 35], depending on the adopted source distance [25, 32]. Diffuse emission is modeled with the standard model for point source analysis `gll_iem_v06.fits` and the corresponding isotropic background.

*Data.* For our analysis, we use almost seven years of ultraclean *Fermi*-LAT P8R2 data taken between August 4 2008 and June 3 2015 (we find similar results for source class data). We select both front- and back converted events in the energy range 1–4 GeV, which covers the peak of the GCE spectrum. The region of interest (ROI) covers the Inner Galaxy and spans Galactic longitudes  $|\ell| \leq 12^\circ$  and latitudes  $2^\circ \leq |b| \leq 12^\circ$ . The data are binned in Cartesian coordinates with a pixel size of  $0.1^\circ$ .

*Wavelet peaks.* The wavelet transform of the  $\gamma$ -ray data is defined as the convolution of the photon count map,  $\mathcal{C}(\Omega)$ , with the wavelet kernel,  $\mathcal{W}(\Omega)$ ,

$$\mathcal{F}_{\mathcal{W}}[\mathcal{C}](\Omega) \equiv \int d\Omega' \mathcal{W}(\Omega - \Omega') \mathcal{C}(\Omega'), \quad (1)$$

where  $\Omega$  denotes Galactic coordinates [38] [note that  $\int d\Omega \mathcal{W}(\Omega) = 0$ ]. The central observable for the current analysis is the *signal-to-noise ratio* (SNR) of the wavelet transform, which we define as

$$\mathcal{S}(\Omega) \equiv \frac{\mathcal{F}_{\mathcal{W}}[\mathcal{C}](\Omega)}{\sqrt{\mathcal{F}_{\mathcal{W}^2}[\mathcal{C}](\Omega)}}, \quad (2)$$

where in the denominator the wavelet kernel is squared before performing the convolution. If the  $\gamma$ -ray flux varied only on scales much larger than the extent of the wavelet kernel, and in the limit of a large number of photons,  $\mathcal{S}(\Omega)$  would behave like a smoothed Gaussian random field. Consequentially,  $\mathcal{S}(\Omega)$  can be loosely interpreted as the local significance for having a source at position  $\Omega$  in units of standard deviations.

As the wavelet kernel, we adopt the second member of the mexican hat wavelet family, which was shown to provide very good source discrimination power [39] and which was used for the identification of compact sources in Planck data [40]. The wavelet can be obtained by a successive application of the Laplacian operator to a two-dimensional Gaussian distribution with width  $\sigma_b R$ .

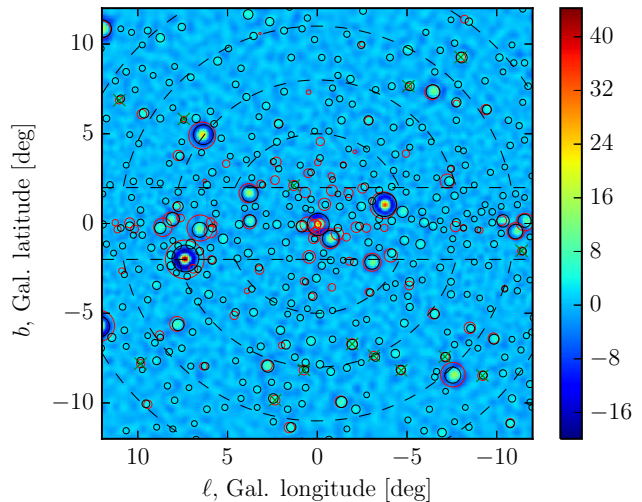


FIG. 1. SNR of the wavelet transform of  $\gamma$  rays with energies in the range 1–4 GeV,  $\mathcal{S}(\Omega)$ . The black circles show the position of wavelet peaks with  $\mathcal{S} \geq 2$ ; the red circles show the position of third Fermi-LAT catalog (3FGL) sources. In both cases, the circle area scales with the significance of the source detection in that energy range. The dashed lines indicate the regions that we use for the binned likelihood analysis, where latitudes  $|b| < 2^\circ$  are excluded because of the strong emission from the Galactic disk. The subset of 3FGL sources that remains unmasked in our analysis is indicated by the green crosses.

Here,  $\sigma_b = 0.4^\circ$  corresponds to the *Fermi*-LAT angular resolution at 1–4 GeV, and  $R$  is a tuning parameter. We find best results when  $R$  varies linearly with latitude from  $R = 0.53$  at  $b = 0^\circ$  to  $R = 0.83$  at  $b = \pm 12^\circ$ . This compensates to some degree the increasing diffuse backgrounds towards the Galactic disk, while optimizing the source sensitivity at higher latitudes [40].

The resulting SNR of the wavelet transform  $\mathcal{S}(\Omega)$  is shown in Fig. 1. As expected, the Galactic diffuse emission is almost completely filtered out by the wavelet transform, whereas bright sources lead to pronounced peaks. We adopt a simple algorithm for peak identification: we find all pixels in  $\mathcal{S}(\Omega)$  with values larger than in the four adjacent pixels. We then clean these results from artifacts by forming clusters of peaks with coplanar distances less than  $0.3^\circ$ , and only keep the most significant peak in each cluster.

In Fig. 1, we show the identified wavelet peaks with peak significance  $\mathcal{S} > 2$ , as well as all 3FGL sources for comparison [1]. For sources that are bright enough in the adopted energy range, we find a good correspondence between wavelet peaks and the 3FGL, both in terms of position and significance (we compare the significance of wavelet peaks  $\mathcal{S}$  with the 1–3 GeV detection significance for sources).

It is worth emphasizing that for the adopted spherically symmetric and centrally peaked distribution of the

CSP, most of the sources would be detected not directly at the GC but a few degrees away from the Galactic disk. This is simply due to the much weaker diffuse emission at higher latitudes. Our focus on latitudes  $|b| \geq 2^\circ$ , thus, avoids regions where source detection becomes less efficient, due to strong diffuse foregrounds, without significant sensitivity loss for the source population of interest.

*3FGL sources.* Before studying the statistics of the wavelet peaks in detail below, we remove almost all peaks that correspond to the known 3FGL sources based on a  $0.3^\circ$  ( $1^\circ$  for  $\sqrt{TS} \geq 50$ ) proximity cut. However, in order to mitigate a potential bias on  $L_{\max}$ , we do not mask peaks that correspond to 3FGL sources that are likely part of the CSP. We identify such *MSP candidate sources* by requiring that they (i) are tagged as unassociated, (ii) show no indication for variability and (iii) have a spectrum compatible with MSPs. The last criterion is tested by performing a  $\chi^2$  fit of the above MSP reference spectrum to the spectrum given in the 3FGL (0.1–100 GeV; five energy bins). Only the normalization is left free to vary. We require a fit quality of  $\chi^2/\text{DOF} \leq 1.22$  (with  $\text{DOF}=4$ ), corresponding to a  $p$  value  $\geq 0.3$ .

We find 13 3FGL sources in the Inner Galaxy ROI that pass the above MSP cuts (listed in the Supplemental Material). Interestingly, the average number of MSP candidate sources in same-sized control regions along the Galactic disk in the range  $|\ell| = 12^\circ\text{--}60^\circ$  is significantly smaller, with an average of 3.1. It is tempting to interpret this excess of MSP candidate sources in the Inner Galaxy as being caused by the brightest sources of the CSP, above the less-pronounced thick-disk population of MSPs [41, 42]. However, we emphasize that the status of these 13 sources is currently neither clear nor qualitatively decisive for our results. Whether we mask them plays a minor role in the detection of the CSP below (but it does affect the inferred values for  $L_{\max}$ ; see Supplemental Material).

*Statistical analysis.* In Fig. 2 we show a histogram of the wavelet peaks in our ROI. We bin the peaks in a two-dimensional grid, which spans the projected angle from the Galactic Center  $2^\circ\text{--}17^\circ$  and wavelet peak significances in the range 1–10. The bin edges are as indicated in the figure. As expected, photon shot noise gives rise to a large number of peaks with low significances  $\mathcal{S} \leq 3$ , and only a small number of peaks has  $\mathcal{S} \geq 5$ .

We assume that the number of peaks in each bin in Fig. 2 follows – in repeated experiments and random realizations of the CSP – to a good approximation a Poisson distribution. We estimate the corresponding average number of expected wavelet peaks in each bin using a large number of Monte Carlo simulations, where we simulate the diffuse background emission, random realizations of the source population and photon shot noise.

In order to quantify what CSP luminosity function reproduces best the observations, we perform a binned

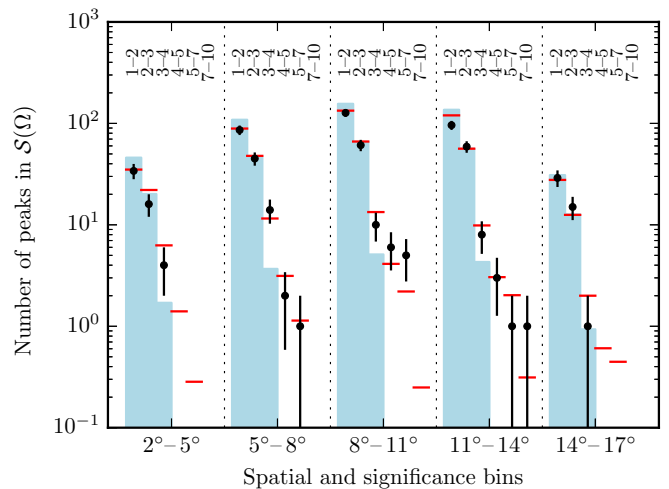


FIG. 2. Histogram of observed peaks in  $\mathcal{S}(\Omega)$ , in bins of projected radial distance from the GC and SNR values (black dots with statistical error bars). We show the expectation value for the case of a negligible CSP as blue bars, whereas the expectation values for the best fit are shown in red.

Poisson likelihood analysis of the wavelet peak distribution. The likelihood function is given by

$$\mathcal{L} = \prod_{i=1}^{n_r} \prod_{j=1}^{n_s} \mathcal{P}(c_{ij} | \mu_{ij}(L_{\max}, \Phi_5)), \quad (3)$$

where  $n_r$  and  $n_s$  are, respectively, the numbers of radial and peak SNR bins,  $c_{ij}$  is the observed and  $\mu_{ij}$  the expected number of peaks, and  $\mathcal{P}$  is a Poisson distribution. The expectation values depend directly on the maximal luminosity,  $L_{\max}$ , as well as on the number of simulated sources,  $n$ . To ease comparison with the literature, we determine  $n$  as a function of  $\Phi_5$ , which denotes the mean differential intensity of the CSP at  $b = \pm 5^\circ$ ,  $\ell = 0^\circ$ , and 2 GeV. In the case of the GCE, this value was found to be  $\Phi_5^{\text{GCE}} = (8.5 \pm 1.5) \times 10^{-7} \text{ GeV}^{-1} \text{ cm}^{-2} \text{ s}^{-1} \text{ sr}^{-1}$  at 95.4% C.L. [15].

*Results.* In Fig. 2, we show the expectation values that we obtain when neglecting contributions from the CSP (and any other nondiffuse emission). This corresponds to good approximation to the case where the GCE is of truly diffuse origin, including the case of DM annihilation or outburst events. We find that the observed number of wavelet peaks with  $\mathcal{S} < 2$  is significantly lower than expected, whereas the observed number of peaks with  $\mathcal{S} > 3$  is significantly higher. As we will show next, this is precisely the effect that is caused by a dim source population.

We now turn to the case with a nonzero CSP contribution. In Fig. 3, we show the limits that we obtain on the two CSP parameters when fitting the histogram in Fig. 2 as described above. We find that a

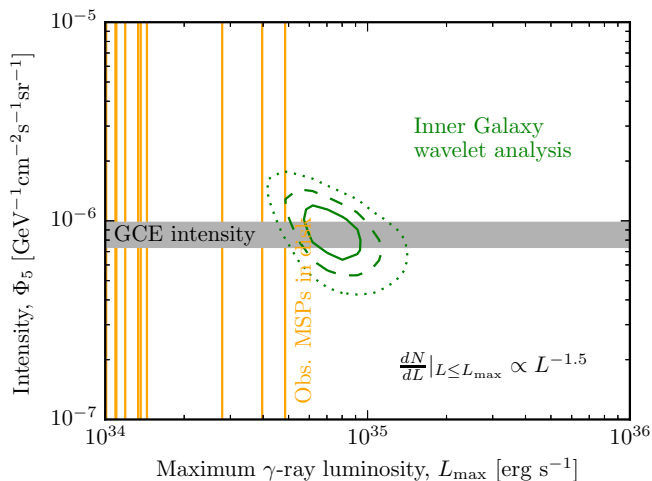


FIG. 3. Constraints on the maximum  $\gamma$ -ray luminosity of the CSP,  $L_{\max}$ , and the population averaged intensity at  $b = \pm 5^\circ$ ,  $\ell = 0^\circ$ , and 2 GeV,  $\Phi_5$ , as derived from our wavelet analysis. We show 68.7%, 95.4%, and 99.7% C.L. contours. We also indicate the values of  $\Phi_5$  where the source population can explain 100% of the GCE (horizontal gray band, 95.4% CL), and as vertical orange lines the luminosity of the brightest observed nearby MSPs.

nonzero contribution from the CSP is favored at the level of at least  $10.0\sigma$  (when quoting the statistical significance, we conservatively take into account bins with  $\mathcal{S} < 5$  only, which are most affected by a dim source population, and least affected by the masking of 3FGL sources [see the Supplemental Material for details]). The best-fit value for the total differential intensity is  $\Phi_5 = (9.0 \pm 1.9) \times 10^{-7} \text{ GeV}^{-1} \text{ cm}^{-2} \text{ s}^{-1} \text{ sr}^{-1}$  and for the maximum luminosity  $L_{\max} = (7.0 \pm 1.0) \times 10^{34} \text{ erg s}^{-1}$ . As can be seen in Fig. 2, we obtain in this case a very good fit to the data.

Our preferred range of the maximum  $\gamma$ -ray luminosities reaches up to  $L_{\max} \leq 1.04 \times 10^{35} \text{ erg s}^{-1}$  (at 95.4% C.L.), which is compatible with observations of nearby MSPs. We illustrate this by showing in Fig. 3 the  $\gamma$ -ray luminosity of the brightest individually observed nearby MSPs as given in Ref. [35] (we only show objects where second  $\gamma$ -ray pulsar catalog [33] distances are available; see Ref. [25] for a detailed discussion about distance uncertainties). Furthermore, for the adopted slope of the luminosity function,  $\alpha = 1.5$ , the best-fit value for the total differential intensity of the CSP  $\Phi_5$  is consistent with the CSP accounting for 100% of the GCE emission.

*Discussion and conclusions.* We found corroborating evidence for the hypothesis that the GCE is caused by a hitherto undetected population of MSP-like sources. We performed a wavelet transform of the  $\gamma$ -ray emission from the Inner Galaxy, which removes Galactic diffuse emission and enhances point sources, and we studied the

statistics of the peaks in this transform. We detected with  $10.0\sigma$  significance a suppression (enhancement) of low- (high-) significance wavelet peaks, relative to the expectations for purely diffuse emission. We showed that this effect is caused by the presence of a large number of dim point sources. The spatial distribution of wavelet peaks in the Inner Galaxy is compatible with a centrally peaked source distribution, and the inferred cutoff of the  $\gamma$ -ray luminosity function of these sources agrees with the observation of nearby MSPs. This source population can, for reasonable slopes of the luminosity function, account for 100% of the GCE emission.

For the purpose of this Letter, which introduces a novel technique, we kept our analysis as simple as possible. In general, one might worry that our results could be affected by the presence of extragalactic and Galactic sources, by the thick-disk population of MSPs and young pulsars, by the details of masking and unmasking 3FGL sources, by the details of the adopted  $\gamma$ -ray luminosity function, and by unmodeled substructure in the Galactic diffuse emission that is not removed by the wavelet transform. We address all of these points in the Supplemental Material and show that it is rather unlikely that they affect our results qualitatively, although quantitative changes in the obtained best-fit values for  $\Phi_5$  and  $L_{\max}$  are possible. In particular, we showed that the wavelet signal expected from the thick-disk population of MSPs is an order of magnitude weaker than what we actually observed and that interpretations related to unmodeled gas remain on closer inspection unlikely.

The prospects for fully establishing the MSP interpretation within the coming decade are very good. Our results suggested that upcoming  $\gamma$ -ray observations with improved angular resolution (planned or proposed  $\gamma$ -ray satellites like GAMMA-400 [43], ASTROGAM, and PANGU [44]) will allow us to detect many more of the bulge sources and study their distribution and spectra. For current radio instruments, it remains rather challenging to detect a MSP population in the bulge [25], but prospects for next-generation instruments are good.

We thank for useful discussions with David Berge, Francesca Calore, Ilias Cholis, Jennifer Gaskins, Dan Hooper, Simona Murgia, Tracy Slatyer, Ben Safdi and Jacco Vink. We thank the *Fermi* Collaboration for providing the public *Fermi* data as well as the *Fermi* Science Tools (v10r0p5). SURFsara is thanked for use of the Lisa Compute Cluster. S.K. and C.W. are part of the VIDi research programme “Probing the Genesis of Dark Matter”, which is financed by the Netherlands Organisation for Scientific Research (NWO). R.B. is part of a GRAPPA-Ph.D. program funded by NWO. Part of this work was performed at the Aspen Center for Physics, which is supported by National Science Foundation Grant No. PHY-1066293.

*Note added in proof.*—Recently, we became aware of

another group studying dim  $\gamma$ -ray sources in the Inner Galaxy, using non-Poissonian photon statistics [45].

\* r.t.bartels@uva.nl

† s.krishnamurthy@uva.nl

‡ c.weniger@uva.nl

- [1] F. Acero *et al.* (Fermi-LAT Collaboration), *Astrophys. J. Suppl.* **218**, 23 (2015).
- [2] M. Su, T. R. Slatyer, and D. P. Finkbeiner, *Astrophys. J.* **724**, 1044 (2010), arXiv:1005.5480 [astro-ph.HE].
- [3] M. Ackermann *et al.* (Fermi-LAT Collaboration), *Phys. Rev. Lett.* **115**, 231301 (2015), arXiv:1503.02641 [astro-ph.HE].
- [4] J.-Q. Xia, A. Cuoco, E. Branchini, and M. Viel, *Astrophys. J. Suppl.* **217**, 15 (2015), arXiv:1503.05918 [astro-ph.CO].
- [5] L. Goodenough and D. Hooper, (2009), arXiv:0910.2998 [hep-ph].
- [6] V. Vitale and A. Morselli (Fermi-LAT Collaboration), (2009), arXiv:0912.3828 [astro-ph.HE].
- [7] D. Hooper and L. Goodenough, *Phys. Lett.* **B697**, 412 (2011), arXiv:1010.2752 [hep-ph].
- [8] D. Hooper and T. Linden, *Phys. Rev.* **D84**, 123005 (2011), arXiv:1110.0006 [astro-ph.HE].
- [9] K. N. Abazajian and M. Kaplinghat, *Phys. Rev.* **D86**, 083511 (2012), arXiv:1207.6047 [astro-ph.HE].
- [10] C. Gordon and O. Macias, *Phys. Rev.* **D88**, 083521 (2013), arXiv:1306.5725 [astro-ph.HE].
- [11] O. Macias and C. Gordon, *Phys. Rev.* **D89**, 063515 (2014), arXiv:1312.6671 [astro-ph.HE].
- [12] K. N. Abazajian, N. Canac, S. Horiuchi, and M. Kaplinghat, *Phys. Rev.* **D90**, 023526 (2014), arXiv:1402.4090 [astro-ph.HE].
- [13] T. Daylan, D. P. Finkbeiner, D. Hooper, T. Linden, S. K. N. Portillo, *et al.*, (2014), arXiv:1402.6703 [astro-ph.HE].
- [14] B. Zhou, Y.-F. Liang, X. Huang, X. Li, Y.-Z. Fan, L. Feng, and J. Chang, *Phys. Rev.* **D91**, 123010 (2015), arXiv:1406.6948 [astro-ph.HE].
- [15] F. Calore, I. Cholis, and C. Weniger, *JCAP* **1503**, 038 (2015), arXiv:1409.0042 [astro-ph.CO].
- [16] M. Ajello *et al.* (Fermi-LAT Collaboration), (2015), arXiv:1511.02938 [astro-ph.HE].
- [17] D. Hooper and T. R. Slatyer, *Phys. Dark Univ.* **2**, 118 (2013), arXiv:1302.6589 [astro-ph.HE].
- [18] W.-C. Huang, A. Urbano, and W. Xue, (2013), arXiv:1307.6862 [hep-ph].
- [19] E. Carlson and S. Profumo, *Phys. Rev.* **D90**, 023015 (2014), arXiv:1405.7685 [astro-ph.HE].
- [20] J. Petrovic, P. D. Serpico, and G. Zaharijas, *JCAP* **1410**, 052 (2014), arXiv:1405.7928 [astro-ph.HE].
- [21] I. Cholis, C. Evoli, F. Calore, T. Linden, C. Weniger, and D. Hooper, (2015), arXiv:1506.05119 [astro-ph.HE].
- [22] D. Gaggero, M. Taoso, A. Urbano, M. Valli, and P. Ullio, (2015), arXiv:1507.06129 [astro-ph.HE].
- [23] K. N. Abazajian, *JCAP* **1103**, 010 (2011), arXiv:1011.4275 [astro-ph.HE].
- [24] Q. Yuan and B. Zhang, *JHEAp* **3-4**, 1 (2014), arXiv:1404.2318 [astro-ph.HE].
- [25] T. D. Brandt and B. Kocsis, *Astrophys. J.* **812**, 15 (2015), arXiv:1507.05616 [astro-ph.HE].
- [26] W. Bednarek and T. Sobczak, *Mon. Not. Roy. Astron. Soc.* **435**, L14 (2013), arXiv:1306.4760 [astro-ph.HE].
- [27] R. Voss and M. Gilfanov, *Astron. and Astroph.* **468**, 49 (2007), astro-ph/0610649.
- [28] K. N. Abazajian and M. Kaplinghat, *Phys. Rev. D* **86**, 083511 (2012), arXiv:1207.6047 [astro-ph.HE].
- [29] K. Perez *et al.*, *Nature (London)* **520**, 646 (2015).
- [30] D. Hooper, I. Cholis, T. Linden, J. M. Siegal-Gaskins, and T. R. Slatyer, *Phys. Rev.* **D88**, 083009 (2013), arXiv:1305.0830 [astro-ph.HE].
- [31] I. Cholis, D. Hooper, and T. Linden, *JCAP* **1506**, 043 (2015), arXiv:1407.5625 [astro-ph.HE].
- [32] J. Petrović, P. D. Serpico, and G. Zaharijas, *JCAP* **1502**, 023 (2015), arXiv:1411.2980 [astro-ph.HE].
- [33] A. Abdo *et al.* (The Fermi-LAT collaboration), *Astrophys. J. Suppl.* **208**, 17 (2013), arXiv:1305.4385 [astro-ph.HE].
- [34] S. K. Lee, M. Lisanti, and B. R. Safdi, *JCAP* **1505**, 056 (2015), arXiv:1412.6099 [astro-ph.CO].
- [35] I. Cholis, D. Hooper, and T. Linden, (2014), arXiv:1407.5583 [astro-ph.HE].
- [36] A. W. Strong, *Astrophys. Space Sci.* **309**, 35 (2007), arXiv:astro-ph/0609359 [astro-ph].
- [37] C. Venter, T. Johnson, A. Harding, and J. Grove, (2014), arXiv:1411.0559 [astro-ph.HE].
- [38] F. Damiani, A. Maggio, G. Micela, and S. Sciortino, *The Astrophysical Journal* **483**, 350 (1997).
- [39] J. Gonzalez-Nuevo, F. Argüeso, M. Lopez-Caniego, L. Toffolatti, J. Sanz, *et al.*, *Mon. Not. Roy. Astron. Soc.* **369**, 1603 (2006), arXiv:astro-ph/0604376 [astro-ph].
- [40] P. Ade *et al.* (Planck), *Astron. Astrophys.* **571**, A28 (2014), arXiv:1303.5088 [astro-ph.CO].
- [41] T. Grgoire and J. Knudsen, *Astron. Astrophys.* **554**, A62 (2013), arXiv:1305.1584 [astro-ph.GA].
- [42] F. Calore, M. Di Mauro, F. Donato, and F. Donato, *Astrophys. J.* **796**, 1 (2014), arXiv:1406.2706 [astro-ph.HE].
- [43] N. Topchiev, A. Galper, V. Bonvicini, O. Adriani, R. Aptekar, *et al.*, *Bull. Russ. Acad. Sci. Phys.* **79**, 417 (2015).
- [44] X. Wu, M. Su, A. Bravar, J. Chang, Y. Fan, *et al.*, *Proc. SPIE Int. Soc. Opt. Eng.* **9144**, 91440F (2014), arXiv:1407.0710 [astro-ph.IM].
- [45] S. K. Lee, M. Lisanti, B. R. Safdi, T. R. Slatyer, and W. Xue, *Phys. Rev. Lett.* **116**, 051103 (2016).
- [46] T. Dame, D. Hartmann, and P. Thaddeus, *Astrophys. J.* **547**, 792 (2001), arXiv:astro-ph/0009217 [astro-ph].
- [47] J.-M. Casandjian, *Astrophys. J.* **806**, 240 (2015), arXiv:1506.00047 [astro-ph.HE].

- [48] We note for reference that for such a MSP, placed at GC distance, we would have seen around 270 photons in our energy range. From this and Tab. I one can estimate that  $\sim 100$  photons correspond to a wavelet signal with a significance of  $S \sim 2$ .
- [49] A. A. Stark and Y.-G. Lee, *Astrophys. J.* **619**, L159 (2005), arXiv:astro-ph/0403631 [astro-ph].

## SUPPLEMENTAL MATERIAL

In the Supplemental Material we discuss the possible impact of various systematic effects on our results. This includes a control region analysis, a discussion of various types of  $\gamma$ -ray sources, substructure in diffuse emission, a thick-disk population of MSPs, sphericity and the role of negative wavelet peaks.

### A. Null results in control regions

In order to estimate the effect of various systematic uncertainties, it is useful to apply our analysis on control regions along the Galactic disk (in the case of Galactic diffuse emission this was first systematically done in Ref. [15]). Potentially unresolved substructure in the Galactic diffuse emission (e.g. in the form of giant molecular clouds, see below), and contributions from various Galactic and extragalactic source populations could be responsible for the detected wavelet signal in the inner Galaxy, but would in general also affect other regions in the Galactic disk. To this end, we focus on (partially overlapping) control regions along the Galactic disk, which are of the same size as the inner Galaxy ROI, but displaced by  $\Delta\ell = \pm k 20^\circ$  with  $k = 1, 2, 3, 4$ .

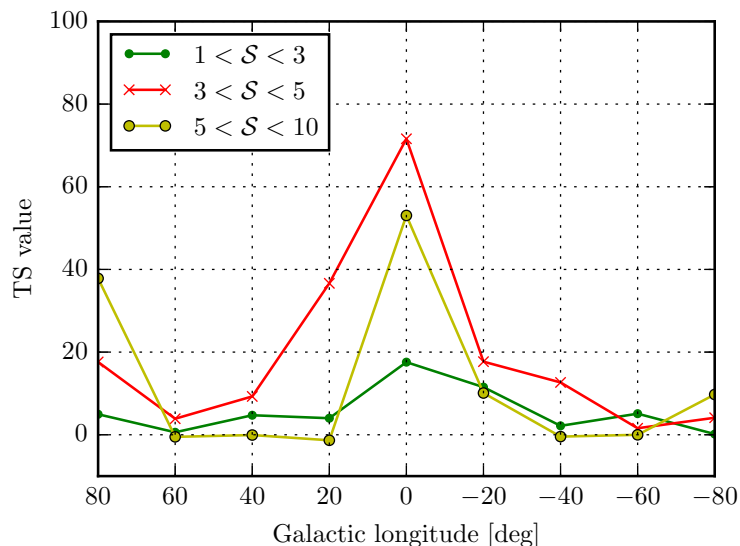


FIG. S-1. We show, as function of the central longitudinal position of the control regions (for  $\ell = 0^\circ$  the main ROI), the significance of a CSP detection. We assume that the CSP is centered in each of the ROIs, and we refit the parameters  $L_{\max}$  and the number of sources. We indicate how different ranges of the wavelet peak significances contribute to the detection. *All* 3FGL sources are masked in this plot, in order to be conservative.

In Fig. S-1 we show the  $TS$  value for a detection of the CSP for the main and the different control ROIs along the Galactic disk. We leave  $L_{\max}$  and  $\Phi_5$  free to vary in each region independently. In the main ROI that covers the inner Galaxy we find the significant detection of a CSP that was discussed in the main text. As shown in the plot, this high significance is supported by the low, intermediate and high-significance SNR peaks of the wavelet transform separately. The directly adjacent regions also show relatively large  $TS$  values, which is either caused by the partial overlap of these control regions with the main ROI, or by a CSP that is more disk-like than assumed in our analysis. We will address the latter point below. However, in the outermost six control regions we find no significant detection of a CSP, for any of the considered values for  $L_{\max}$  and  $\Phi_5$  (the large  $TS$  values at  $\ell = 80^\circ$  are caused by one extremely bright source that generates fake peaks in its tails). This observation makes it already extremely unlikely that our findings are driven by a mismodelling of the local Galactic diffuse emission, or by extragalactic sources. We will address this in more detail below.

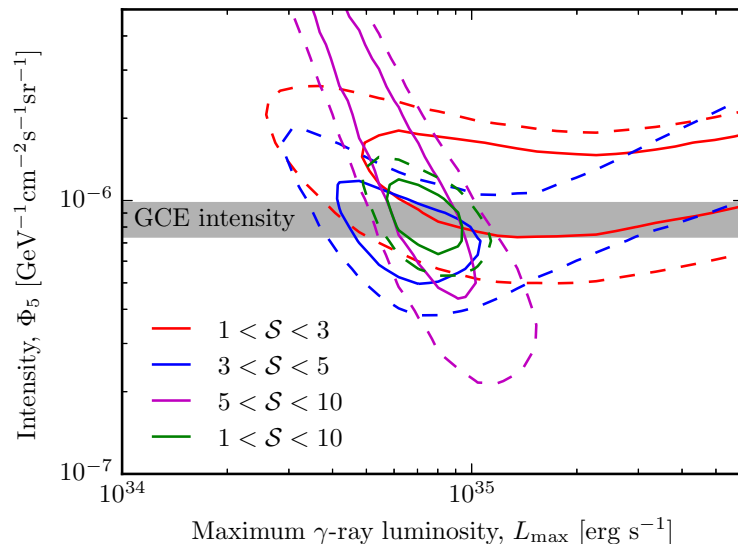


FIG. S-2. Similar to Fig. 3 in the main text, but showing limits derived for different ranges of the wavelet peak significances separately. The parameter degeneracies present in some of the fits cancel when fitting the entire significance range at once. We only show 68.7% and 95.4% CL constraints for clarity.

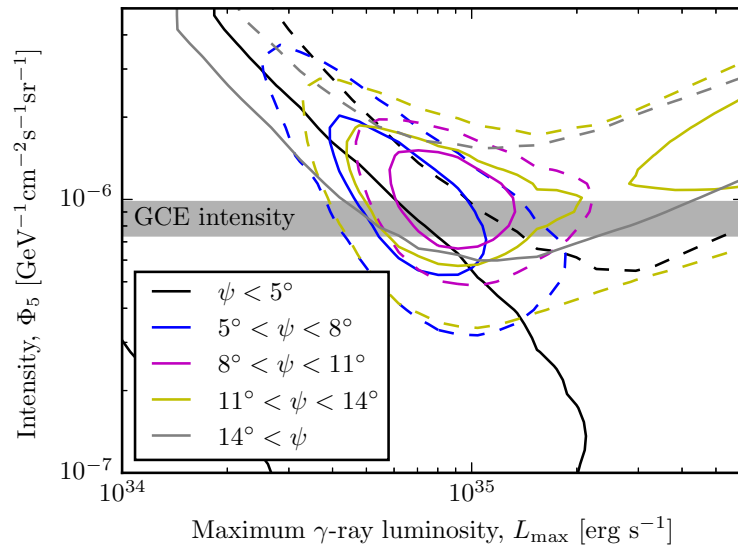


FIG. S-3. Similar to Fig. 3 in the main text, but showing limits as derived for different spatial bins separately.

### B. Consistent wavelet signal in separate bins

It is instructive to see how wavelet peaks with different significances contribute to the constraints on the luminosity function that we showed in Fig. 3 in the main text. To this end, we show in Fig. S-2 the limits that we obtain separately from peak significances in the range  $\mathcal{S} = 1-3$ ,  $\mathcal{S} = 3-5$  and  $\mathcal{S} = 5-10$ , respectively. All three constraints are mutually consistent to within  $1\sigma$ , leading to a consistent interpretation of the peaks shown in Fig. 1 in the main text. In all cases we find some degeneracy in the  $(L_{\max}, \Phi_5)$  plane. High significance peaks predominantly provide a stringent upper limit on  $L_{\max}$ , whereas low significance peaks mostly constrain the overall luminosity of the modelled source population.

To show that our assumption on the spatial distribution of the CSP is consistent with the data, we show Fig. S-3

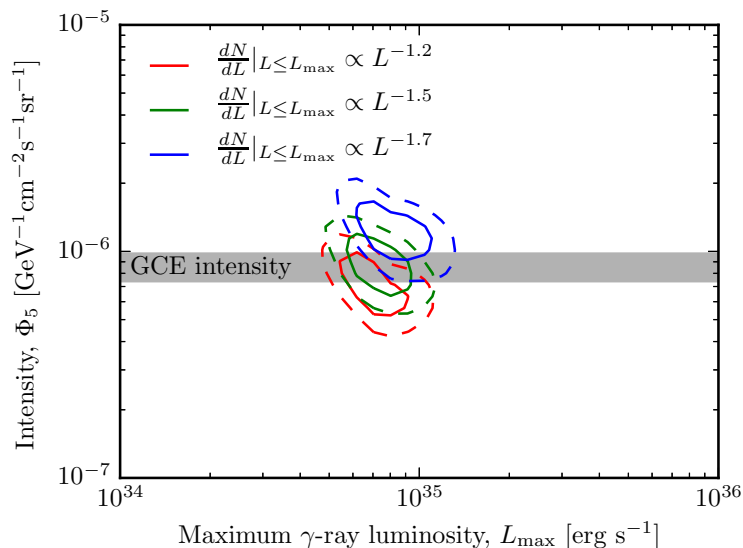


FIG. S-4. Similar to Fig. 3 in the main text. We show the 68.7% and 95.4% CL contours for luminosity functions with spectral indices of 1.2, 1.5 and 1.7.

the result obtained for the five different spatial bins independently. Ring 1–5 correspond to  $r \in [i^\circ, i + 3^\circ]$  with  $i = 2, 5, 8, 11, 14$ , respectively. We find constraints on  $L_{\max}$  and  $\Phi_5$  that are mostly consistent to within  $1\sigma$ .

Finally, we checked that the identified wavelet peaks are symmetrically distributed in the north, south, east and west parts of our main ROI. Only at  $S > 3$  we find a slight (statistically not very significant) asymmetry with more peaks in the south, which might be caused by the somewhat stronger Galactic foregrounds in the north, which makes point source detection in the north more challenging.

### C. Mild dependence on the MSP luminosity function

Theoretically,  $\alpha$  is not well constrained and can plausibly range from 1.5 to 3, depending on the emission model [32, 36, 37]. Actual MSP observations actually seem to indicate somewhat smaller values closer to  $\alpha \sim 1.2$  [35]. We show in Fig. S-4 the 68.7% and 95.4% CL contours for different luminosity functions, respectively with spectral indices of 1.2 and 1.7. For a fixed intensity ( $\Phi_5$ ), hardening (softening) of the luminosity function corresponds to an enhancement (suppression) of the number of sub-threshold point sources, which explains the direction in which the best fit region moves. We note that we obtain very similar  $TS$  values for all slopes that we considered.

### D. The role of unmasked 3FGL sources

In the present analysis, we make use of the 3FGL, the third *Fermi* source catalogue, which is based on the first four years of *Fermi* pass 7 data. One important ingredient in our analysis is the masking of 3FGL sources. These sources are of Galactic and extragalactic origin and leaving them unmasked would inevitably induce sizeable signals in our search for a sub-threshold source population in the bulge. However, as discussed in the main text, we keep unassociated sources with MSP-like spectra unmasked. These sources could be part of the bulge MSP population that we are looking for, and masking them would bias our results. The 13 sources that pass our MSP cuts are listed in Tab. I.

In general, falsely masking unassociated sources that actually belong to the bulge MSP population would push  $L_{\max}$  to lower values, whereas falsely unmasking foreground sources would push it to large values. This is illustrated in Fig. S-5. We show the case where we mask *all* unassociated sources, as well as the case where we adopt a weaker criterion for the spectral fit, leaving around 20 sources unmasked. We find that in both cases the best-fit value for  $L_{\max}$  moves in the expected direction, but the results remain consistent to within  $1\sigma$ . Furthermore, the significance of our wavelet detection that we quote in the main text (where we include  $\mathcal{S} < 5$  bins only) changes to  $9.2\sigma$  when we

3FGL Name	$\ell$ [°]	$b$ [°]	$\chi^2/\text{dof}$	$\sqrt{TS}$	$\mathcal{S}$	$L$ [ $10^{34}$ erg/s]
J1649.6-3007	-7.99	9.27	1.07	5.6	7.4	$7.8^{+5.5}_{-2.7}$
J1703.6-2850	-5.08	7.65	0.48	2.4	5.0	$3.4^{+2.4}_{-1.2}$
J1740.5-2642	1.30	2.12	0.37	6.4	3.5	$14.9^{+10.6}_{-5.1}$
J1740.8-1933	7.43	5.83	0.77	1.9	2.3	$3.8^{+2.7}_{-1.3}$
J1744.8-1557	11.03	6.88	0.40	3.7	3.4	$5.6^{+3.9}_{-1.9}$
J1758.8-4108	-9.21	-8.48	0.90	5.6	3.8	$4.8^{+3.4}_{-1.7}$
J1759.2-3848	-7.11	-7.43	0.35	4.6	5.6	$5.9^{+4.2}_{-2.0}$
J1808.3-3357	-1.94	-6.71	0.40	6.9	6.3	$8.0^{+5.7}_{-2.7}$
J1808.4-3519	-3.15	-7.36	0.41	4.6	4.4	$5.0^{+3.5}_{-1.7}$
J1808.4-3703	-4.68	-8.19	0.22	4.9	5.3	$4.3^{+3.1}_{-1.5}$
J1820.4-3217	0.74	-8.17	1.04	5.7	1.7	$7.2^{+5.1}_{-2.5}$
J1830.8-3136	2.35	-9.84	0.54	5.9	6.0	$5.0^{+3.6}_{-1.7}$
J1837.3-2403	9.85	-7.81	0.28	4.0	3.0	$4.7^{+3.3}_{-1.6}$

TABLE I. List of the 13 unassociated 3FGL sources with MSP-like spectra, which we leave unmasked in our analysis. If the GeV excess is caused by dim point sources, it is likely that some or most of them are part of the CSP. The last four columns show the goodness-of-fit of the reference MSP spectrum, the 3FGL significance in the 1–3 GeV band, the corresponding peak of the wavelet SNR, and the  $\gamma$ -ray luminosity (assuming  $8.5 \pm 2$  kpc distance from the source and the reference stacked MSP spectrum from the main paper with a normalization that is obtained from a fit to the measured source flux).

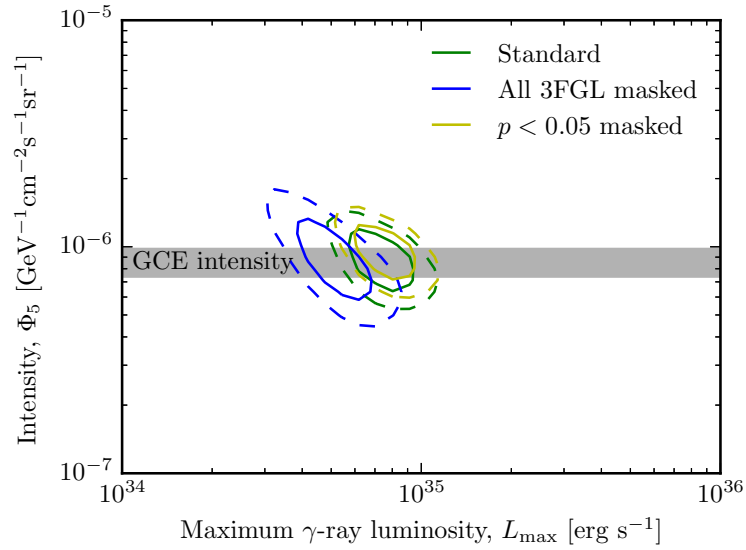


FIG. S-5. Similar to Fig. 3 in the main text. We show the effect of masking *all* 3FGL sources, or leaving a slightly larger number unmasked.

mask all sources, and to  $10.8\sigma$  when keeping 20 sources unmasked. The (un-)masking of 3FGL is hence not decisive for our qualitative findings, although quantitative results can be affected.

It is interesting to note that the faintest 3FGL source in the inner Galaxy ROI that passes our MSP-spectrum cut, has a luminosity of  $L = 3.4 \times 10^{34}$  erg s $^{-1}$  if placed at 8.5 kpc distance. This is a good, though rough, indication for the *de facto* sensitivity threshold of *Fermi*-LAT for the detection of sources with MSP-like spectra in the bulge region.

Lastly, one can use the sources in Tab. I to compare the sensitivity of the 3FGL with our wavelet analysis. Averaging over the 13 sources, we find a ratio of  $\mathcal{S}/\sqrt{TS} \simeq 1.0 \pm 0.4$ , indicating that the sensitivity of the wavelet method is similar to the 3FGL sensitivity in a comparable energy range. However, the scatter exceeds the one expected from statistical fluctuations alone, which can be attributed to differences in the systematics that affect the 3FGL and the wavelet analysis.

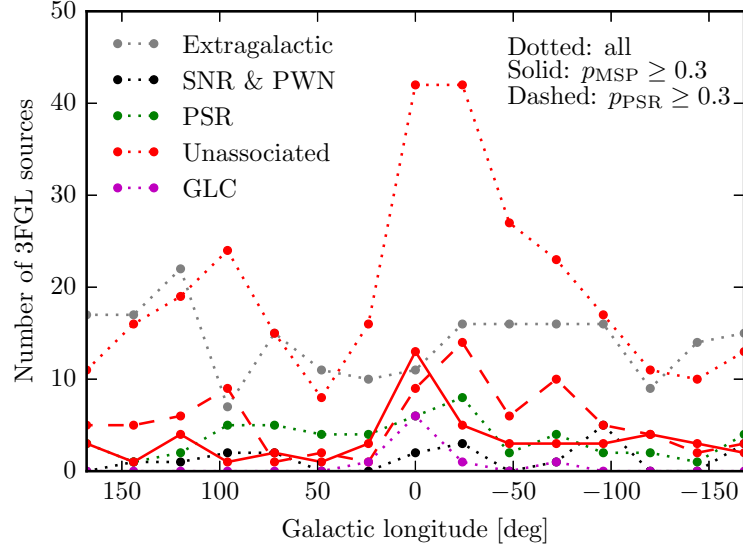


FIG. S-6. Latitude profile of sources, for different ROIs along the Galactic disk, as function of their longitudinal center (dotted lines). The ROIs have a size of  $24^\circ \times 24^\circ$ , with the Galactic disk,  $|b| < 2^\circ$ , masked. The different colors correspond to different source categories. In the case of unassociated sources, the solid (dashed) lines show only sources that pass the spectrum cut for MSP-like (young pulsar-like) sources.

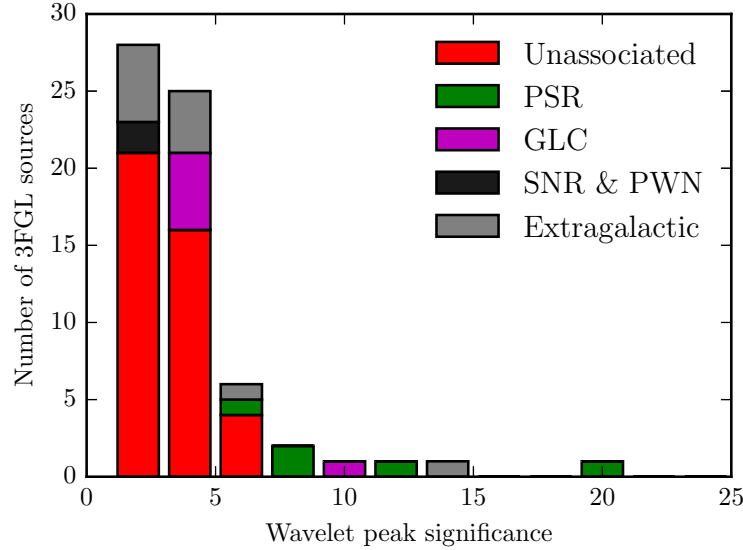


FIG. S-7. Stacked histogram of wavelet peak values  $S$  that correspond to 3FGL sources in the inner Galaxy ROI. We show the contribution from different source categories separately. Unassociated sources generate mostly low-significance wavelet peaks, whereas for example source that are marked as pulsar in the 3FGL only generate peaks with a high significance (see discussion).

### E. The role of various source populations

In Fig. S-6, we show the number of 3FGL sources in our inner Galaxy ROI as well as in various same-sized ROIs that are displaced along the Galactic disk in steps of  $\Delta\ell = \pm 24^\circ$ . We show (identified and associated) extragalactic sources, various Galactic source classes and unassociated sources classes separately. We also show for the unassociated sourced how many sources pass our MSP cut. It is apparent that the number of unassociated sources strongly peaks in the inner Galaxy ROI, however with a clear asymmetry towards negative values of  $\ell$ , and another peak around  $\ell \approx 100^\circ$ . However, after applying the MSP cut, predominantly sources in the inner Galaxy survive. In Fig. S-7, on

the other hand, we show a histogram of the wavelet peak significance that our analysis attributes to the 3FGL sources in the inner Galaxy ROI. Again, unassociated sources play a major role and produce wavelet peaks down to values of  $\mathcal{S} \sim 1$ . On the other hand, 3FGL sources that are identified as pulsars appear only with  $\mathcal{S} > 5$  in our analysis. We will discuss in the following the potential impact of each of the source classes separately.

*Extragalactic sources.* As shown in Fig. S-6, the number of extragalactic sources in the individual ROIs along the Galactic disk fluctuates around values of about  $\sim 13$ . No significant suppression is observed in the inner Galaxy ROI, which would have indicated that it is more challenging to identify or associate extragalactic sources in this region. We will use here a simple argument to show that extragalactic sources cannot play a significant role for our results. The average number of  $\mathcal{S} = 3-5$  wavelet peaks in the above control regions along the Galactic disk is 20; in the inner Galaxy ROI it is 42 (we exclude here *all* 3FGL sources to be conservative). If extragalactic sources were the main contribution to these peaks, in addition to the about 10 wavelet peaks that are expected from statistical fluctuations alone (see Fig. 2 in the main text), the 42 observed peaks would constitute a  $> 5\sigma$  upward fluctuation above the expected 20. This makes it extremely unlikely that extragalactic sources contribute significantly to our results in the inner Galaxy. Similar arguments can be made using wavelet peaks in the range  $\mathcal{S} = 1-2$ .

*Supernova remnants and pulsar wind nebulae.* As apparent in Fig. S-6, only a very small number of sources along the Galactic disk at latitudes  $|b| > 2^\circ$  (and almost none at  $|b| > 5^\circ$ ) are identified with supernova remnants or pulsar wind nebulae. In our ROIs their number is much less than the number of extragalactic sources, and their distribution is centrally not peaked, indicating that sources at these latitudes are mostly local. Sources in this category are typically more easily detectable at higher and lower energies than the energy range used in our analysis, and would be most likely listed in the 3FGL and hence masked if they were abundant and significant. We consider it hence as extremely unlikely that sources of this category significantly affect our results in the inner Galaxy.

*Young and millisecond pulsars.* An interesting feature of pulsars in the 3FGL is that they always induce large wavelet signals in our analysis, as shown in Fig. S-7. This makes indeed sense, since the identification of a  $\gamma$ -ray source as pulsar requires the measurement of its pulsation, and hence a large enough number of photons. Furthermore, the pulsar energy spectrum often peaks close the energy range of our analysis. Already from Fig. S-7 it is obvious that a large fraction of the unassociated sources, which mostly appear with lower significance peaks, must in fact be pulsars. Interestingly, as shown in Fig. S-6, identified pulsars do not show a centrally peaked distribution, whereas the unassociated sources clearly do. This behaviour is expected, given that with increasing distance the pulsar identification becomes more challenging.

*Globular clusters.* The  $\gamma$ -ray emission from globular clusters that is not masked in our analysis, either because the globular clusters did not enter the 3FGL, or because they happen to be among our 13 unmasked unassociated sources, could in principle contribute to the detected signal. Since their total emission is usually due to several MSPs which appear as a single source for *Fermi*-LAT, their presence could bias  $L_{\max}$  towards larger values. However, given the simulation results from Ref. [25], we expect this effect to be small, and leave a more detailed discussion to future work.

*Unassociated sources.* The peak of unassociated sources in the inner Galaxy, as shown in Fig. S-6, appears clearly asymmetric, with a second peak at  $\ell \approx 100^\circ$ . As discussed above, a large fraction of these sources is expected to be young or millisecond pulsars. Obviously, the 3FGL unassociated sources do not directly contribute to our results since they are masked (except the 13 MSP candidates). However, the unassociated sources are extremely abundant even down to  $\mathcal{S} \sim 1$ , and their probable nature can be used as an indicator for what source population dominates just below threshold.

In Fig. S-6, we see that our MSP cut removes most of the unassociated sources, but leaves an excess of 13 unassociated sources in the inner Galaxy, as discussed above. What is more, if we slightly modify the spectral criterion, using  $dN/dE \propto e^{-E/2 \text{ GeV}} E^{-2}$ , which is somewhat more pulsar-like (softer index, lower cutoff), this behaviour changes and we instead find excesses that are more correlated with the peaks of the unassociated sources away from the inner Galaxy. Although the statistical significance of this finding is rather difficult to quantify without a detailed study (which we leave for future work), this result is indicative. It suggests that a large fraction of the inner Galaxy unassociated (and sub-threshold) sources are likely MSPs, whereas unassociated sources in other parts of the disk have a larger fraction of young pulsars. The latter point is further supported by the fact that similar structures can be found in the longitudinal distribution of identified pulsars.

In summary, we expect that our wavelet signal is dominated by whatever source class is responsible for most of the unassociated sources towards the inner Galaxy. Very likely, these are millisecond and young pulsars, with a somewhat higher MSP/young pulsar ratio than in the rest of the disk. Since these sources appear in general both in the Galactic disk as well as in the bulge, it is important to study whether the excess/suppression of wavelet peaks in the inner Galaxy points to a disk population, a bulge population, or to a combination of both. This will be discussed in the

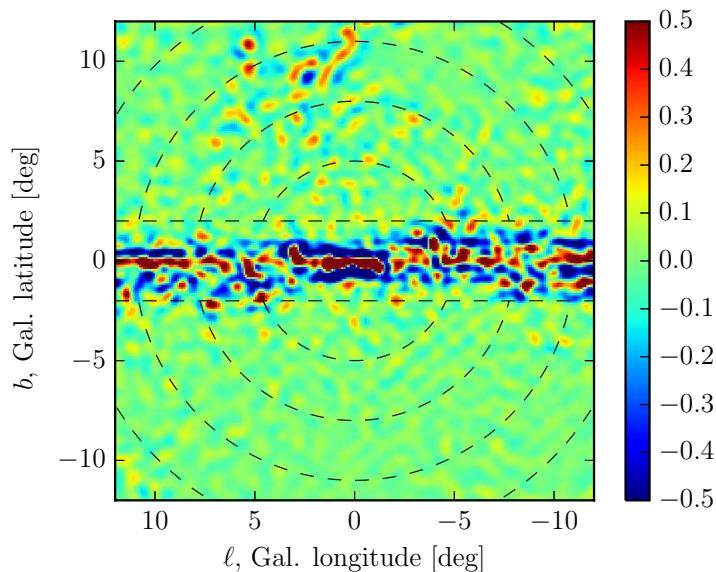


FIG. S-8. Similar to Fig. 1 in the main text (note the different color scale), but showing the transform of the diffuse BG model only, without Poisson noise being applied. Outside of the Galactic disk,  $|b| > 2^\circ$ , which we exclude from our analysis, the significance of wavelet peaks remains below 0.5. The variance is below 0.1, which shows that even  $1\sigma$  peaks in the wavelet transform are unlikely to be strongly affected by the Galactic diffuse emission.

section G below.

### F. Possible caveats concerning the Galactic diffuse emission

In our Monte Carlo studies, we use the standard *Fermi* diffuse model for pass 8 data analysis. The wavelet transform of this model, *without applying Poisson noise*, but using the same exposure as in our main analysis, is shown in Fig. S-8. Outside of the masked Galactic disk at  $|b| > 2^\circ$ , we do not find any excesses with a significance larger than about  $0.5\sigma$ . The main effect of such variations would be to offset the significance of random statistical fluctuations and sub-threshold point sources towards higher or lower values. This would not significantly affect peaks with a large SNR. However, it can potentially be important for low-significance peaks, because the collective shift of a large number of peaks, even by a small amount, could become statistically relevant. But since the variance of the SNR values shown in Fig. S-8 is below 0.1, we do not expect that the details of the modeling of diffuse emission when doing MCs is going to affect our results.

The *Fermi* diffuse models might not actually contain all relevant small-scale gas structures, and the effect of these missing structures on our results is not straightforward to estimate without a detailed analysis and modeling of the power-spectrum of gas at small scales. It is hence rather important that our non-detection of strong wavelet signals along the Galactic disk in Fig. S-1 largely excludes that mismodeling of *local* gas is the cause for the detected signal towards the inner Galaxy, since it would affect other parts of the disk as well. This is in particular true since there is relatively little molecular gas in our main ROI, compared to the control regions [46]. Thus, gas-related effects should be larger in the control regions than in the main ROI.

If one insists on a gas-related interpretation, our results hence suggest that the wavelet signals are caused by unmodeled gas in the Galactic bulge, at a height of 0.3–1.5 kpc. If we assume a cosmic-ray density in the bulge similar to the local one, the differential  $\gamma$ -ray emissivity at 1 GeV is around  $3 \times 10^{-26} \text{ s}^{-1} \text{ GeV}^{-1}$  per hydrogen atom [47]. This implies that dense gas clouds with masses around  $3 \times 10^5 M_\odot$  would be at 1 GeV roughly as bright as MSPs with a luminosity of  $L = 7 \times 10^{34} \text{ erg s}^{-1}$ . [48] Interestingly, giant molecular clouds are known objects of that mass, and they can be dense enough to appear at GC distance point-like for *Fermi*. However, the scale height of known giant molecular clouds is at the level of a few 10 pc (they usually intersect with the Galactic disk) instead of the required  $\sim 1$  kpc [49]. Furthermore, clouds of that size should give rise to CO emission in the range  $\mathcal{O}(10\text{--}100) \text{ K km s}^{-1}$ , which is not seen in current observations [46]. If observed, such CO emission should be distributed

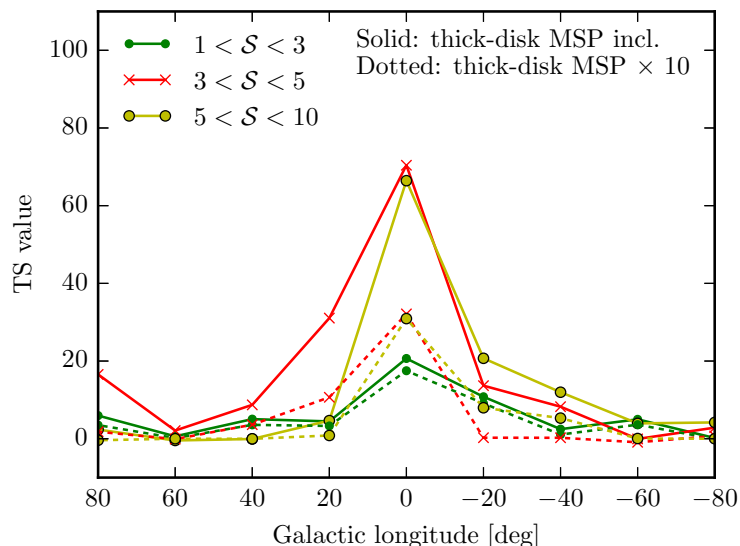


FIG. S-9. Similar to Fig. S-1, but including a thick-disk MSP population calibrated to local bright high-latitude MSPs as additional background. Only for illustration, we also show the effect of a  $10\times$  more dense thick-disk population (which is in contradiction with local observations). Note that we unmask 3FGL as described in the main analysis when deriving the wavelet peaks.

north/south symmetric, as our wavelet peaks are too.

If one could show that a large number of such giant molecular clouds (or other structures with similar mass and density) can form and be transported to kpc heights in the Galactic bulge, while hiding from all observations, the interpretation of the identified wavelet peaks in terms of unmodeled gas would remain a possibility. However, as of now, and for all of the above reasons, we regard gas-related interpretations of our results as rather unlikely and speculative.

### G. Potential impact of thick-disk population

As argued above, the most relevant Galactic background in our ROI are expected to be pulsars, and in particular the MSP thick-disk population that reaches up to high latitudes. We will now show that a thick-disk population of MSPs (or other sources with a similar luminosity function) cannot be responsible for the observed signal.

In most cases, the thick-disk population of MSPs is modeled as a cylindrically symmetric exponential distribution, with a scale height in the range 0.5–1 kpc and a scale radius of a few kpc, which is only poorly constrained by data (see *e.g.* Ref. [41]). We will adopt here a distribution with a scale height of 1 kpc and a scale radius of 5 kpc, which was previously used to argue against the MSP-origin of the *Fermi* GeV excess [31]. The distribution reads  $n \propto \exp(-R/R_s) \exp(-|z|/z_s)$ , with  $R_s = 5$  kpc and  $z_s = 1$  kpc. We will address below how the results change when other parametrizations are adopted.

As  $\gamma$ -ray luminosity function, we adopt an inverse power-law with  $L_{\min} = 10^{31} \text{ erg s}^{-1}$ ,  $L_{\max} = 7 \times 10^{34} \text{ erg s}^{-1}$  and index  $\alpha = 1.5$ . We fix the overall normalization of the disk source density such that the number of bright MSPs at high latitudes,  $|b| > 15^\circ$ , is consistent with the number of such MSPs listed in the 3FGL. As flux threshold for bright MSPs we adopt a flux that corresponds to a  $\gamma$ -ray luminosity of  $10^{34} \text{ erg s}^{-1}$  at 3 kpc distance ( $9.2 \times 10^{-12} \text{ erg s}^{-1} \text{ cm}^{-2}$  in our energy range). We find 31 MSPs above that threshold flux and note that since the number of unassociated high-latitude bright nonvariable sources with a curved enough spectrum is small, this number cannot increase by more than 50% when more unassociated sources are identified as MSPs [1]. For the present scenario, we find that the total number of thick-disk sources with  $\gamma$ -ray luminosity above  $10^{31} \text{ erg s}^{-1}$  is  $\sim 30000$ .

Within 2 kpc of the Galactic center, this thick-disk population predicts around 1300 MSPs, which is more than an order of magnitude below the number that we find in the best-fit scenario for the bulge population (around 35000 MSPs above  $10^{31} \text{ erg s}^{-1}$ ). This implies, as already argued in Ref. [31], that a thick-disk population with the adopted geometry cannot be responsible for the *Fermi* GeV excess. However, it also trivially implies that the number of

wavelet peaks caused by thick-disk sources in the inner 2 kpc is about an order of magnitude below what is predicted by our best-fit bulge population, and hence an order of magnitude below what is actually observed. This still leaves the possibility that thick-disk MSPs on the line-of-sight towards the inner Galaxy, outside of the inner  $\sim 2$  kpc, could affect our results. We will discuss this next.

Within our ROI, the thick-disk population predicts 3.3 sources outside of the inner 2 kpc with a flux in the range  $(4.6\text{--}7.7) \times 10^{-12} \text{ erg s}^{-1} \text{ cm}^{-2}$  (this corresponds roughly to  $(4\text{--}7) \times 10^{34} \text{ erg s}^{-1}$  when the sources are put at 8.5 kpc distance). These sources could reasonably contribute to wavelet peaks in the  $3 < \mathcal{S} < 5$  range. The actually observed number of peaks in that range above the null hypothesis is about 35. It is hence clear that foreground sources from the above thick-disk population cannot cause the observed signal. One might think of two ways around.

First, one could reduce the scale radius of the thick-disk population such that the number of sources in the inner 2 kpc increases by a factor around ten (scale radii around 1–2 kpc could do the job). This would give rise to a wavelet signal similar to what is observed. However, such a population would also predict a significant diffuse  $\gamma$ -ray emission similar to the level of the *Fermi* GeV excess, just with a morphology that is incompatible with the observations. A population with a scale radius of 1–2 kpc would indeed commonly be referred to as bulge population. Such a population would be very similar to the bulge population that we put forward in the main part of the paper as explanation for the *Fermi* GeV excess, with the main difference being that our population fits better the excess morphology.

Second, one could increase the number of MSPs in a ring-like region around the Galactic bulge, excluding the inner 2 kpc, such that these additional ring-like distributed sources will enhance the number of foreground sources without affecting the number of sources in the Galactic bulge. In this case, however, the wavelet signal should clearly be more extended along the Galactic disk than what is shown in Fig. S-1, since such a ring would not be centrally peaked and extend to longitudes of at least  $\sim 25^\circ$ . For illustration, we here quote the relative number of wavelet peaks one expects in the control regions along the disk and the main ROI produces by such a ring (1 kpc scale height, 5 kpc scale radius, the inner 2 kpc radius excluded):  $\Delta\ell = \{\pm 80, \pm 60, \pm 40, \pm 20, 0\}$  and  $N_{\text{peaks}} \propto \{1.7, 2.4, 3.5, 4.9, 3.6\}$ . Moreover, in order to avoid a conflict with the above calibration with bright high-latitude sources, the ring should be further constrained to lie within  $\lesssim 5$  kpc, which however would still leave a too flat central distribution of wavelet peaks.

Finally, we show in Fig. S-9 how the TS values are affected if the thick-disk population (or a  $10\times$  denser population) is added as an additional background component. For simplicity, we assume that the thick-disk population causes deviations of the expectation values  $\mu_{ij}$  in Eq. (3) from the null hypothesis that are proportional to the deviations caused by the best-fit bulge population. We adjust the normalization of these deviations such that the number of additionally predicted  $3 < \mathcal{S} < 5$  peaks in the main ROI is 3.3 (as motivated by the above discussion). We then add these thick-disk-induced deviations from the null hypothesis as negative and positive contributions to the model predictions in Eq. (3), and repeat the CSP fit to inner Galaxy data. We repeat this procedure in all of the control ROIs used in Fig. S-1, reweighing the thick-disk contribution properly at different Galactic longitudes. From Fig. S-9 it is clear that only a thick disk ten times denser than what is actually observed at higher latitudes could significantly affect, although not completely remove, the excess of wavelet peaks in the inner Galaxy.

## H. Further discussions

In order to test whether the spatial distribution of wavelet peaks in our analysis is indeed compatible with a spherically symmetric distribution, we re-binned the wavelet peaks into a north/south region, defined by  $12^\circ > |b| > \max(|\ell|, 2^\circ)$ , and an east/west region, defined by  $12^\circ > |\ell| > |b| > 2^\circ$ . For each of the two regions, we derive the best-fit values for  $L_{\text{max}}$  and  $\Phi_5$ . The results are shown in Fig. S-10. We find that the inferred parameters are consistent within one sigma, with a slightly stronger signal in the north/south region. This indicates that the excess of wavelet peaks, if interpreted in terms of a bulge source population, is consistent with a spherical distribution of these sources.

Given that unresolved sources only add positively to the Galactic diffuse emission, whereas a mismodeling of the gas could cause both positive and negative variations, it is tempting to think that a detection of negative wavelet peaks would disfavour an interpretation in terms of unresolved point sources. In fact, we do find a suppression of  $-2 < \mathcal{S} < -1$  peaks, and an enhancement of  $-4 < \mathcal{S} < -3$  peaks in the inner ROI when searching for negative instead of positive peaks. But unfortunately, this cannot easily be used to discriminate diffuse modeling artefacts (which, as we discussed above, are anyway unlikely, as they should show up in the entire disk) from sub-threshold point sources.

Maybe somewhat un-intuitively, negative wavelet peaks can indeed be generated by a large number of weak, positive point sources. This happens in the tails of our simulated sources, where the wavelet transform becomes negative (this

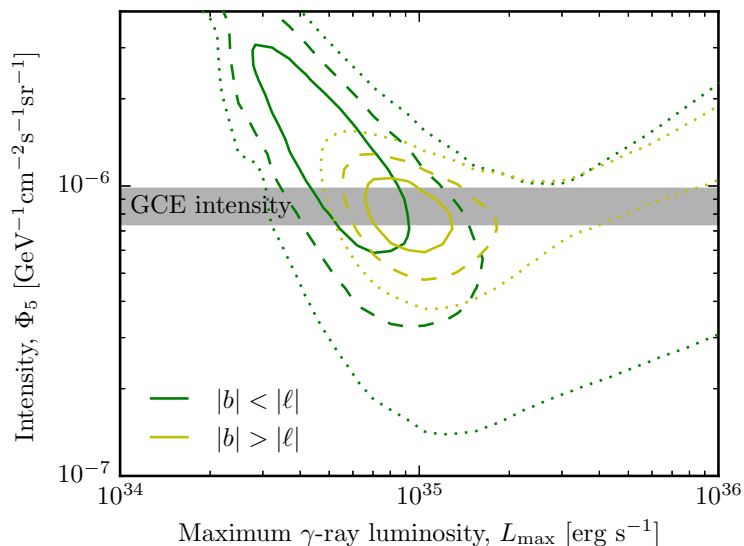


FIG. S-10. Similar to Fig. 3 in the main text, but derived in redefined regions within our main ROI that are useful to check for the sphericity of the signal (we still mask  $|b| < 2^\circ$ ). We find best-fit parameters for  $L_{\max}$  and  $\Phi_5$  in the north/south and east/west regions that are consistent within one sigma.

effect is visible as rings around bright sources in Fig. 1). We estimated the expected number of *negative* wavelet peaks for the best-fit scenario in Fig. 3 by Monte Carlo simulations, and find results that are completely consistent with the observed number of negative peaks. However, given that the number of positive and negative wavelet peaks are correlated (they are caused by the same sources), one cannot easily use observations of negative wavelet peaks to further constrain the model parameters. This, and the fact that an appropriate masking of 3FGL sources (including also the ring around each source) reduces significantly the effective size of the ROI, make an efficient use of negative peaks in our analysis difficult. However, it is re-ensuring that both the observed negative and positive wavelet peaks are consistent with the respective predicted number of negative and positive wavelet peaks for the same sub-threshold point source population.

Finally, we briefly comment on the recent analysis of the Galactic center data by the *Fermi*-LAT collaboration [16] and compare their use of wavelets to ours. Ref. [16] uses wavelets to find seeds for the identification of point sources (also see Ref. [38] for details about the adopted method), followed by standard maximum-likelihood fits for further source identification. This can be potentially affected by interstellar emission modelling. We instead study the statistics of local-maxima in the wavelet-transformed sky map, which is largely background-model independent (although small scale fluctuations could in principle be relevant, as discussed above). We find good correspondence between our wavelet peaks and the 3FGL catalogue (see Fig. 1), which supports the validity of our approach. However, we also find that this agreement and the quality of the wavelet analysis in general critically depends on the adopted wavelet type and size. All these points make it difficult to directly compare our results with those of Ref. [16]. However, we note that the Galactic disk, where Ref. [16] finds that their identified sources most strongly trace the edges of the interstellar emission and thus might constitute false positives due to gas fluctuations (see their Fig. 8), is masked in our analysis.